Mon. Not. R. Astron. Soc. **295**, L41–L44 (1998)

A complete infrared Einstein ring in the gravitational lens system B1938 + 666

L. J. King,[1] N. Jackson,[1] R. D. Blandford,[2] M. N. Bremer,[3] I. W. A. Browne,[1] A. G. de Bruyn,[4,5] C. Fassnacht,[2] L. Koopmans,[4] D. Marlow[1] and P. N. Wilkinson[1]

[1] *University of Manchester, NRAL Jodrell Bank, Macclesfield, Cheshire SK11 9DL*
[2] *California Institute of Technology, Pasadena, CA 91125, USA*
[3] *Institut d'Astrophysique de Paris, 98bis Blvd Arago, 75014 Paris, France*
[4] *Netherlands Foundation for Radio Astronomy, Postbus 2, 7990AA Dwingeloo, the Netherlands*
[5] *Kapteyn Astronomical Institute, Postbus 800, 9700AV Groningen, the Netherlands*

Accepted 1998 January 30. Received 1998 January 30; in original form 1997 October 15

ABSTRACT

We report the discovery, using NICMOS on the *Hubble Space Telescope*, of an arcsec-diameter Einstein ring in the gravitational lens system B1938 + 666. The lensing galaxy is also detected, and is most likely an early-type galaxy. Modelling of the ring is presented and compared with the radio structure from MERLIN maps. We show that the Einstein ring is consistent with the gravitational lensing of an extended infrared component, centred between the two radio components.

Key words: galaxies: active – galaxies: individual: B1938 + 666 – gravitational lensing.

1 INTRODUCTION

In 1992, Patnaik et al. (1992a) published the first results of the Jodrell Bank–VLA Astrometric Survey (JVAS). The primary purpose of the JVAS was to survey flat-spectrum radio sources from the 5-GHz NRAO catalogues (Condon & Broderick 1985; Condon & Broderick 1986; Condon, Broderick & Seielstad 1989), in order to identify phase reference sources for MERLIN. Six gravitational lens systems have been found in this survey: B0218 + 357 (Patnaik et al. 1993), MG0414 + 0534 (this object was originally discovered in the MIT–Greenbank survey; Hewitt et al. 1992), B1422 + 231 (Patnaik et al. 1992b), B1030 + 074 (Xanthopoulos et al. 1998), B2114 + 022 (Augusto, Wilkinson & Browne 1996), and B1938 + 666 (Patnaik et al. 1992a; King et al. 1997), the subject of this paper.

B1938 + 666 has a complex radio structure, with a dominant arc and two pairs of fairly compact components contained within an arcsec separation (Patnaik et al. 1992a; King et al. 1997). The contours on Fig. 1 show the 5-GHz MERLIN radio map. King et al. (1997) provide a simple model of the system, in which the lensed object consists of three components. The first component (R2) lies in the three-image region of the source plane, is compact, has a steep spectrum, and produces a double radio image separated by about 1 arcsec. The second (R1) and third components both lie in the five-image region, producing four detectable images. (The third component is a weak component close to R1 and will not be included in the models presented here; see Fig. 2.) Two images, one of R1 and one of the third component, combine to form a relatively compact condensation at the southern end of the system.

Rhoads, Malhotra & Kundić (1996) reported infrared and optical imaging observations of B1938 + 666, taken at the Apache Point Observatory. They detected an object coincident with the radio position of the lens system, with a very red optical–infrared colour [$r(0.65\ \mu m) - K'(2.12\ \mu m) = 6.8 \pm 0.25$]. The angular resolution of their observations was not high enough to determine whether the object detected was the lensing galaxy or the lensed source.

2 *HST* OBSERVATIONS AND RESULTS

Observations of B1938 + 666 were obtained on 1997 August 13 with the Near Infrared Camera/Multi-Object Spectrograph (NICMOS) attached to the *Hubble Space Telescope*. Four observations, of 3840, 1088, 3840 and 2048s, were obtained, giving a total integration time of just over three hours over two orbits of spacecraft time.

The NIC-1 camera was used for these observations, which has a pixel scale of 43 mas and a resolution of approximately

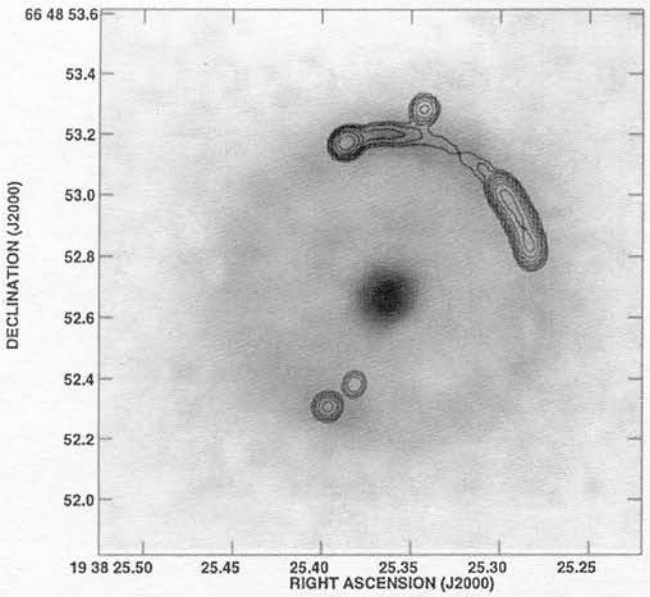

Figure 1. The 5-GHz MERLIN map of B1938 + 666 (logarithmic contours with the lowest contour at 0.5 mJy beam^{-1}), and the NICMOS picture as a grey-scale.

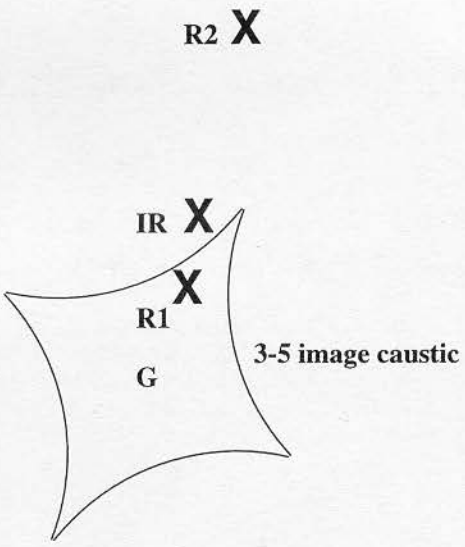

Figure 2. A schematic for the source plane of B1938 + 666, with crosses indicating the intrinsic positions of the radio components R1 and R2 and the infrared component IR, with respect to the three–five image caustic. The lensing galaxy centre is marked G, and is 51 mas from the radio component R1. the infrared component IR is extended all the way into the caustic; the parts that lie close to the middle of the caustic produce the ring. Component R1 produces the arc complex at the northern end of the radio structure, together with the most southerly compact component; R2 is doubly imaged, producing the two compact components outside the ring. See fig. 6 of King et al. (1997) for a more detailed description of how the radio components map on to the image plane.

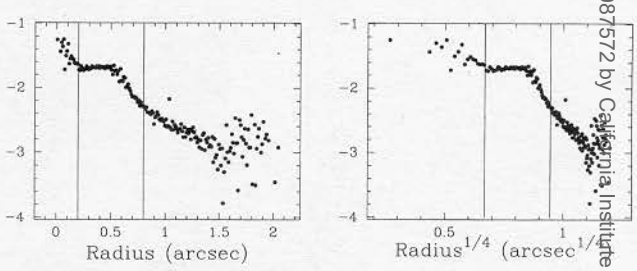

Figure 3. Surface brightness profiles in the image, plotted on a log scale, against r and $r^{1/4}$, where r is the distance from the centre of the lensing galaxy. The regions between $r = 0.2$ and 0.8 arcsec (indicated by vertical lines) are contaminated by emission from the ring.

the diffraction limit of 0.14 arcsec. The F160W filter was used, which has a peak wavelength of 1.583 μm and a FWHM of 0.40 μm, and corresponds approximately to the standard infrared *H* band. All observations were calibrated by the standard STScI pipeline procedure involving bias and dark current subtraction, linearity and flat-field correction, photometric calibration and cosmic ray identification and removal. All observations were taken using MULTIACCUM mode, which consists of multiple non-destructive readouts of the detectors. This allows good cosmic ray detection and removal. The final image has been formed by co-addition of the four individual exposures and rotated using the ORIENTAT keyword in the file header.

Only one, quite complex, object is visible in the ∼11-arcsec field of view (shown as a grey-scale on Fig. 1). This object consists of a central condensation, surrounded by a ring of diameter 0.95 arcsec. More extended fuzz is also visible out to a radius of ∼2 arcsec. We identify the central condensation as the centre of the lensing galaxy, and the extended fuzz as its outer regions. The lensing galaxy has a compact, bright core and low ellipticity. In Fig. 3 we show, following Driver, Windhorst & Griffiths (1995), the light profiles (on a log scale) integrated over all angles (as a major-axis cut has very low signal-to-noise ratio) and plotted against r (exponential disc), the distance from the centre of the lensing galaxy, and against $r^{1/4}$ (de Vaucouleurs). Unfortunately, the combination of high noise at the outer radii and the ring emission does not allow an unambiguous determination of the lensing galaxy type,[1] although the profile roughly fits the de Vaucouleurs $r^{1/4}$ profile and the morphology is suggestive of the Driver et al. (1995) E/S0 types.

The lensed object is extended in the optical, and some part of it is lensed into the ring structure that we see in the *HST* picture. We present and discuss more detailed models of the system below.

The total *H* magnitude of all components visible is measured as 18.0 ± 0.3 (of which the lensing galaxy contributes 18.6 ± 0.3) with an error dominated by the relatively bright and variable background. Because of the rough agreement with the *H* magnitude obtained by Rhoads et al. (1996), 17.6 ± 0.1, and because no other object is visible in our field,

[1]The formal χ^2 is slightly greater for the de Vaucouleurs profile than for the exponential disc, but large errors are introduced by the high and variable background.

it is likely that the object seen in the *HST* image is the same as the Rhoads et al. (1996) identification.

3 LENS MODEL AND DISCUSSION

In this section we show that the Einstein ring and ring-peaks in the NICMOS picture of B1938 + 666 are consistent with the gravitational lensing of an infrared source close to the radio sources. This is achieved though lens modelling and comparison of the infrared and radio structures.

The lens models were obtained using the NRAO AIPS task GLENS (see the AIPS Cookbook for details), which models the action of a gravitational lens on a background source. We do not use a more complex lens modelling algorithm in this paper because our primary aim is to show that the appearance of B1938 + 666 on the NICMOS picture can be attributed to lensing, and also because the source and lens redshifts remain undetermined. In GLENS, the lens was represented by an isolated elliptical potential well of the asymptotically isothermal form discussed by Blandford & Kochanek (1987), the projected centre of which in the source plane was specified by a pixel position. Unlensed source components were represented by circular Gaussians and were also assigned pixel positions in the source plane. The position and magnification of images formed when a source is lensed are related to the first and second derivatives of the lensing potential respectively; see for example Blandford & Kochanek (1987).

We used GLENS to obtain a simple lens model for the 5-GHz MERLIN map of B1938 + 666, using the model and multifrequency observations presented in King et al. (1997) as a starting point. The MERLIN map was made using the Caltech package DIFMAP procedure (Shepherd 1997). The source plane was divided into a 512×512 grid, with each pixel corresponding to 3.1 mas in the source plane. The critical radius of the lens (b) was set to 465 mas; this quantity is related to the velocity dispersion of the lens (σ) and the ratio of the lens–source to observer–source angular diameter distances, D_{LS}/D_{OS}, through $b = 4\pi(\sigma/c)^2 D_{LS}/D_{OS}$. For the lensing galaxy the ellipticity, ϵ, was fixed at a modest value of 0.07, which is consistent with the Einstein ring and the appearance of the lensing galaxy itself on the NICMOS picture. The position angle of the major axis of the galaxy (N through E) was fixed at 150°, which results in a good radio (and NICMOS) image model. The main features on the radio map were reproduced by representing the unlensed source by two Gaussian components and iteratively varying the positions of the component, running GLENS and comparing the image-plane output with the 5-GHz map. We convolved the image-plane output for our best model to a resolution similar to the 5-GHz MERLIN map (which has a beam of 47×44 mas in PA = −9°) using the AIPS task CONVL. Fig. 2 indicates the positions of the primary radio components R1 and R2 with respect to the three–five image caustic.

To obtain a model for the NICMOS picture we used the same parameters to describe the lensing galaxy as in the radio model. What do we know about the infrared source that would be lensed to reproduce the features of the NICMOS picture? There are two main peaks in the ring on the NICMOS picture, consistent with a source centred in the three-image region of the source plane, close to radio component R2. If the infrared emission was centred in the five-image region coincident with R1, there would be a strong peak at a position angle similar to that of the arc complex observed in the radio map. That there is a complete ring in the NICMOS picture suggests that the source of the infrared emission is much larger than that of the radio emission. Our initial model for the unlensed source therefore consisted of a Gaussian centred on the position of R2, covering the three–five image caustic.

The positional accuracy of NICMOS is about 0.5 arcsec, so we cannot directly identify corresponding positions in the radio map and NICMOS picture, although the radio arc must straddle the critical line that corresponds to the image of the caustic separating the three–five image regions and also traces the position of the Einstein ring. To correct for the discrepancy between the radio and optical reference frames, the radio model and map were superimposed and J2000 coordinates corresponding to the pixel position of the lens were determined. As the position of the lens was the same in the radio and optical models and the lens is visible on the NICMOS picture, it can be used to fix the optical coordinate reference frame. In Fig. 1 we show the radio map as contours with the NICMOS picture as a grey-scale.

When the initial NICMOS image model was put on the same coordinate frame as the NICMOS picture, the peaks in the model and picture had a small offset. We corrected for this by moving the model infrared source slightly closer to the three–five image caustic (marked IR on Fig. 2); Fig. 4 shows the NICMOS picture (contours) and image model (grey-scale). This produces good agreement between the

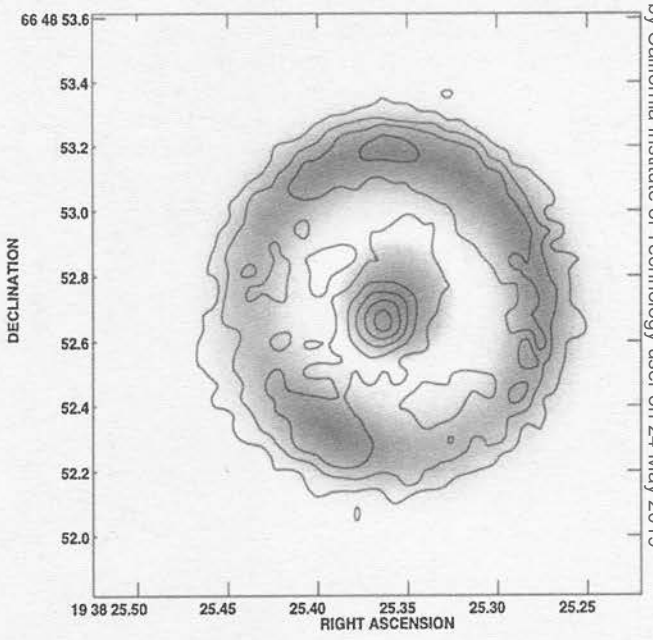

Figure 4. The NICMOS picture of B1938 + 666 (contoured at 0.01×2, 2.5, 3, 4, 5, 6, 7, 8 counts s^{-1}) and the GLENS NICMOS image model as a grey-scale. Note that the central blob of the image model corresponds to the position of the lensed object in the absence of lensing, whereas the central bright object in the NICMOS picture corresponds to the lensing galaxy.

model and the observed NICMOS images. It should be noted that they grey-scale image includes a representation of the unlensed source at its centre. The NICMOS picture itself reveals the lensing galaxy slightly displaced from the position of the unlensed source, as expected. The relative positions of the radio components and the infrared source as required by the model, shown in Fig. 2, indicate that the background object is a compact radio galaxy; the radio lobes are disposed symmetrically on either side of the host galaxy.

The magnitude of the lensed source is ~ 19 in H, giving it an intrinsic magnitude of ~ 21.5 in H, because it is likely to be magnified by a factor of about 10 (see e.g. the formula of Refsdal & Surdej 1994). This is likely to correspond to $K \sim 22.5$, fainter by about 3 magnitudes than typical brightnesses of radio galaxies at $z = 2$ (Dunlop et al. 1989). This low magnitude may be a consequence of reddening in the lensing galaxy, which could be tested by *HST* observations using WFPC2 to determine the optical–infrared colours of the lensed source and lensing galaxy. Further high-sensitivity radio observations may reveal a radio core coincident with the infrared counterpart.

The lensing galaxy has an infrared magnitude similar to that of the galaxies of Dunlop et al. at $z \sim 1$–2. If the ratio $D_{LS}/D_{OS} = 0.5$, then $\sigma = 180$ km s^{-1} for the lensing galaxy. If the lensing galaxy is an L_* elliptical ($\sigma = 220$ km s^{-1}), then D_{LS}/D_{OS} is smaller, consistent with the lens being closer to the source, which is also suggested by the infrared magnitude of the lensing galaxy.

4 SUMMARY

We have discovered an infrared Einstein ring in the lens system B1938 + 666, using NICMOS on the *HST*. The lensing galaxy is also detected well above the noise. We have compared the infrared and radio structures, and demonstrated that the ring is consistent with the gravitational lensing of an extended component, probably a galaxy, centred between the two main radio components. More detailed modelling and *HST* imaging in other wavebands will pin down the properties of the lensing galaxy and the intrinsic positions of the radio and infrared components.

ACKNOWLEDGMENTS

This research used observations with the *Hubble Space Telescope*, obtained at the Space Telescope Science Institute, which is operated by Associated Universities for Research in Astronomy Inc. under NASA contract NAS5-26555. MERLIN is operated as a National Facility by NRAL, University of Manchester, on behalf of the UK Particle Physics & Astronomy Research Council. This research was supported in part by European Commission, TMR Programme, Research Network Contract ERBFMRXCT96-0034 'CERES'. We thank Mark Lacy and Hanadi AbdelSalam for useful discussions. LJK is grateful to the Astrophysics Department, University of Oxford, for hospitality during part of the writing of this paper.

REFERENCES

Augusto P., Wilkinson P. N., Browne I. W. A., 1996, in Kochanek C. S., Hewitt J. N., eds, IAU Symp. 173, Astrophysical Applications of Gravitational Lensing. Kluwer, Dordrecht, p. 399
Blandford R. D., Kochanek C. S., 1987, ApJ, 321, 658
Condon J. J., Broderick J. J., 1985, AJ, 90, 2540
Condon J. J., Broderick J. J., 1986, AJ, 91, 1051
Condon J., Broderick J. J., Seielstad G. A., 1989, AJ, 97, 1064
Driver S. P., Windhorst R. A., Griffiths R. E., 1995, ApJ, 453, 48
Dunlop J. S., Guiderdoni B., Rocca-Volmerange B., Peacock J A., Longair M. S., 1989, MNRAS, 240, 257
Hewitt J. N., Turner E. L., Lawrence C. R., Schneider D. P., Brody J. P., 1992, AJ, 104, 968
King L. J., Browne I. W. A., Muxlow T. W. B., Narasimha D., Patnaik A. R., Porcas R. W., Wilkinson P. N., 1997, MNRAS, 289, 450
Patnaik A. R., Browne I. W. A., Wilkinson P. N., Wrobel J. M., 1992a, MNRAS, 254, 655
Patnaik A. R., Browne I. W. A., Walsh D., Chaffee F. H., Foltz C. B., 1992b, MNRAS, 259, 1
Patnaik A. R., Browne I. W. A., King L. J., Muxlow T. W. B., Walsh D., Wilkinson P. N., 1993, MNRAS, 261, 435
Refsdal S., Surdej J., 1994, Rep. Prog. Phys., 57, 117
Rhoads J. E., Malhotra S., Kundić T., 1996, AJ, 111, 642
Shepherd M. C., 1997, Astron. Data Anal. Software Syst., 6, 77
Xanthopoulos E. et al., 1998, MNRAS, saubmitted